01 Jan 2023

Cascaded Sapphire Fiber Bragg Gratings Inscribed By Femtosecond Laser For Molten Steel Studies

Dinesh Reddy Alla

Deva Prasad Neelakandan

Farhan Mumtaz
Missouri University of Science and Technology, mfmawan@mst.edu

Rex E. Gerald
Missouri University of Science and Technology, geraldr@mst.edu

et. al. For a complete list of authors, see https://scholarsmine.mst.edu/ele_comeng_facwork/5183

Recommended Citation

D. R. Alla et al., "Cascaded Sapphire Fiber Bragg Gratings Inscribed By Femtosecond Laser For Molten Steel Studies," *IEEE Transactions on Instrumentation and Measurement*, Institute of Electrical and Electronics Engineers, Jan 2023.
The definitive version is available at https://doi.org/10.1109/TIM.2023.3335530

Cascaded Sapphire Fiber Bragg Gratings Inscribed by Femtosecond Laser for Molten Steel Studies

Dinesh Reddy Alla, Deva Prasad Neelakandan, Farhan Mumtaz, *Member, IEEE*, Rex E. Gerald II, Laura Bartlett, Ronald J. O'Malley, Jeffrey D. Smith, and Jie Huang, *Senior Member, IEEE*

***Abstract*— This research reports a distributed fiber optic high-temperature sensing system tailored for applications in the steel industry and various other sectors. Recent advancements in optical sensor technology have led to the exploration of sapphire crystal fibers as a solution for sensing in harsh environments. Utilizing a femtosecond (fs) laser, cascaded fiber Bragg gratings (FBGs) were meticulously fabricated within a multimode sapphire optical fiber. These FBGs endowed the system with distributed sensing capabilities and underwent rigorous testing under extreme temperatures, reaching up to 1800 °C. The study delves into the investigation of the FBG reflection spectrum, facilitated by the development of a sophisticated multimode demodulation system, which contributed to the attainment of precise temperature measurements with a performance accuracy of 99.9%. Demonstrating exceptional thermal stability, the sapphire FBGs endured temperatures of 1600 °C for a sustained duration of 22 h. Furthermore, this article explores the application of distributed temperature sensing employing multiple sapphire FBGs, showcasing their utility in temperature measurements related to molten steel studies.**

***Index Terms*— Femtosecond (fs) laser, fiber Bragg gratings (FBGs), fiber sensors, molten steel, sapphire optical fiber, submerged entry nozzle (SEN).**

I. Introduction

In 2022, the United States observed the production of approximately 94.7 million net tons of steel, marking a significant milestone with substantial ramifications for the energy sector [1]. Small improvements in operating stability, efficiency, and product yield translate to substantial energy cost savings for the industry on an annual basis. The annual total energy expenditures in the U.S. steel industry exceed six billion dollars. A 10% enhancement of energy efficiency would lead to 600 million dollars in savings per year in the U.S. steel industry [2]. The production of 1 ton of crude steel generates about 1.9 tons of carbon dioxide. The improvement of production efficiency and the elimination of waste will also lead to a significant reduction in carbon dioxide emissions. Distributed temperature measurements at various molten steel processing stages will lead to an increase in production efficiency and a reduction in energy requirements.

In steel manufacturing, several areas in the continuous casting process would benefit from distributed temperature measurement at steelmaking temperatures. One such area is the submerged entry nozzle (SEN), which is the refractory component that transfers the liquid steel from the tundish to the mold, protects the steel from air exposure, and directs the steel flow in a controlled manner in the mold. A distributed temperature sensor array placed within the SEN wall could be used for submergence control, SEN wear monitoring, monitoring of wave activity and flow asymmetry in the mold, and continuous steel temperature monitoring in the mold. Such measurements would enable improvements in quality, safety, and production efficiency in the continuous casting process.

In recent years, fiber optic sensors have proven to be valuable sensing systems with higher accuracy, high measurement resolution, and wide sensing range compared to thermocouples. One of the commercially available and commonly used fiber-optic sensors was the FBGs [3], [4]. Various applications of FBGs for measuring strain and temperature in industries were widely discussed [5], [6]. In recent years, the application of FBGs for temperature measurements in the steel industry has been extensively reported [7], [8], [9], [10]. Lieftucht et al. [8] successfully developed a continuous caster mold monitoring system through temperature measurements using FBGs, known as a high-definition mold (HD mold). Later, Wans et al. [7] described the improvement in process stability and enhancement in product quality obtained by monitoring the heat transfer in an HD mold, which provided sufficient time for the operator to take actions necessary correct anomalous casting conditions. In 2018, Castiaux et al. [9] reported an efficient way of installing FBGs in copper molds and evaluated their potential for thermal mapping of liquid steel and breakout detection of mold during steel casting.

Conventional FBGs are developed through an ultraviolet (UV) laser-based phase mask method, where the optical fiber undergoes type-I refractive index modulation. However, the type-I index modulated FBGs typically have low operating temperatures (<450 °C). Another solution was to use a femtosecond (fs) laser to fabricate FBGs through a point-by-point method. The fs laser creates type-II refractive index modulation along the optical fiber and can withstand extremely harsh environments and that can measure high temperatures (∼1800 °C) [11], [12], [13], [14], [15], [16]. In the last decade, Mihailov et al. [13] reported various applications of fs-laser

Manuscript received 17 July 2023; revised 6 October 2023; accepted 1 November 2023. Date of publication 28 November 2023; date of current version 26 December 2023. This work was supported in part by the Peaslee Steel Manufacturing Research Center (PSMRC) and in part by the U.S. Department of Energy's Office of Energy Efficiency and Renewable Energy (EERE) under the Advanced Manufacturing Office (AMO) under Award DE-EE0009119. The Associate Editor coordinating the review process was Dr. Yuya Koyama. *(Corresponding author: Jie Huang.)*

Dinesh Reddy Alla, Farhan Mumtaz, Rex E. Gerald II, and Jie Huang are with the Department of Electrical and Computer Engineering, Missouri University of Science and Technology, Rolla, MO 65409 USA (e-mail: jieh@mst.edu).

Deva Prasad Neelakandan, Laura Bartlett, Ronald J. O'Malley, and Jeffrey D. Smith are with the Department of Material Science and Engineering, Missouri University of Science and Technology, Rolla, MO 65409 USA.

Digital Object Identifier 10.1109/TIM.2023.3335530

fabricated FBGs in harsh and extreme environmental conditions. The fs laser fabricated single-mode silica FBGs have provided efficient and accurate sensing means for temperatures $<$1200 °C, but for temperatures beyond 1200 °C, sapphire optical fiber-based sensors would provide a viable option for accurate temperature sensing. Sapphire crystal fibers possess remarkable attributes, including an exceptionally high melting point exceeding 2072 °C, excellent transparency within the telecommunication band, resistance to corrosion, and immunity to electromagnetic interference [17], [18], [19]. Wang et al. [18] discussed sapphire optical fiber-based ultrahigh temperature sensing systems based on FBGs, interferometry, Raman scattering, and sapphire thermometry principles. Unlike silica-based optical fibers, the sapphire fibers are fabricated in the shape of semi-cylindrical rods without a layer of cladding, and with commercially available fiber diameters, the beam propagation in the optical fiber is highly multimodal at the near-infrared telecommunication bands.

Sapphire optical fiber thermometry was a single-point temperature sensing system that uses thermal radiation from a sapphire optical fiber for temperature sensing [18], [20], [21], [22]. Qian et al. [22] successfully demonstrated a nanorod alumina-coated sapphire fiber-based optical fiber thermometer for temperature analysis in molten steel. However, the sensing principle was based on the intensity analysis of thermal radiation spectra, which can be affected by ambient light coupling and variations in fiber position. To overcome these issues, a convolution neural network algorithm was developed and trained for temperature classification from the thermal radiation spectra.

The fs-laser inscribed sapphire FBGs are reported to be stable, efficient, and effective for harsh environments and ultrahigh-temperature measurements [23], [24], [25]. Habisreuther et al. [23] reported a fs-laser fabricated air-clad sapphire FBG for temperature measurements in the range of 1900 °C along with FBG multiplexing for distributed sensing. The fs laser fabricated sapphire FBGs based on phase masks for temperature and strain sensing were previously discussed [15], [26], [27]. Busch et al. [26] reported the fs-laser phase mask fabricated sapphire FBG for temperature measurements in the range of 1750 °C along with a long-term test with temperatures cycling between 1200 °C and 500 °C for 120 h. The commercially available sapphire optical fibers are highly multimodal; hence, the fs laser line-by-line scanning method was commonly applied for FBG fabrication, which resulted in higher reflectivity [28], [29], [30], [31] over the point-by-point fabrication method [17], [32]. Xu et al. [28] investigated fs laser-based line-by-line fabricated FBGs reflectivity and SNR change compared to FBGs fabricated at different layers and layer spacings within the diameter of the fiber. The line-by-line-based fabrication method has resulted in sapphire FBGs with greater reflectivity.

Despite the highly reflective sapphire FBGs, most of the reported sapphire FBG spectra exhibit poor signal-to-noise ratio (SNR), distorted peaks, low fringe visibility, and broad linewidth. These issues are mainly due to the highly multimodal interference of the air-cladded sapphire optical fibers. Efforts have been made to address these issues, including the investigation of proper cladding materials to minimize the number of modes [33], the fabrication of a near-single mode sapphire optical fiber [32], and the use of an ultralong lead-in optical multimode fiber to reduce the multimodal interference [23], [27], [31], [34]. The cladded sapphire optical fibers have shown reduced numerical apertures, but most of the cladding materials can only withstand up to 1400 °C due to the mismatch in the thermal expansion coefficients of the coating and sapphire materials. The near-single mode sapphire optical fiber can be a good solution but with a drastically reduced diameter that may degrade the mechanical strength of the fiber. An ultralong lead-in optical multimode fiber can reduce the multimodal interference to some extent but still cannot drastically minimize it. Moreover, rigorous packaging of the lead-in fiber was also required. In summary, there remains a strong need for the development of sapphire FBGs exhibiting high-quality reflection spectra and a novel interrogation unit to eliminate multimodal interference. In a recent contribution, our research group has reported [35], [36], [37] the successful fabrication of large-scale cascaded multimode FBGs through the meticulous first-order point-by-point technique. These FBGs were constructed within sapphire crystal fiber and coreless fiber, and they demonstrated exceptional fringe visibility ranging up to $\sim$6 dB. This high fringe visibility characteristic represents a significant advantage for the realization of distributed thermal mapping in the context of sensing in the harsh environments.

In telecommunications for spatial multiplexing, higher order modes are excited in multimode fibers by fabricating specialized 3-D tapers, which selectively excite required modes eliminating multimode interference [38], [39], [40]. Lai et al. [39] reported a silicon-based spot size converter made from tapered channel waveguides and a Y-junction, which reduced coupling loss at higher order modes. In 2020, Weihong shen et al. [40] reported a silicon-integrated edge coupler, which contains a triple tip inverse taper in a multimode fiber for building an efficient integrated multimode interface for simultaneous coupling of two modes into the fiber for mode division multiplexing.

In this article, we report the fs laser-based sapphire FBG fabrication through a line-by-line scanning method, which results in high reflectivity, good SNR, a low full-width at half-maximum (FWHM), and a thermal stability of long duration. A novel mode scrambler method was also included in the interrogation unit to drastically minimize the multimode interference of sapphire optical fiber. The FBG was tested at temperatures of up to 1800 °C and, for the first time to the best of our knowledge, the fiber was employed for measurements in molten steel by embedding the fiber into an alumina-graphite SEN refractory to monitor temperature during the direct immersion of the refractory into molten steel. This innovative sensing technology holds immense potential for continuous temperature monitoring in the demanding environments of steel molds, refractory components, furnaces, turbine engines, and boilers [17], [41], [42], [43].

II. Theory

FBGs can be manufactured using either single-mode or multimode optical fibers. In single-mode fibers, only the fundamental mode is guided, leading to a simpler design and analysis of the Bragg grating. Conversely, multimode

fibers support multiple modes, which adds complexity to the design and analysis of the Bragg grating. When light travels through a multimode fiber, it excites multiple modes, each with distinct velocities and phase accumulations over a specific distance. Consequently, the power distribution among these modes varies along the length of the fiber, creating an opportunity to create a multimode FBG. The reflectivity of the grating in a multimode FBG can be expressed as [36]

$$R(L,\lambda) = \frac{\sum_{\sigma} |\chi_{0\sigma}|^2 \zeta_{\sigma}}{\sum_{\sigma} |\chi_{0\sigma}|^2} \tag{1}$$

where $\chi_{0\sigma}$ and ζ_{σ} denote the incident modal amplitude and modal reflectivity, respectively. L represents the length of the grating, while λ stands for the operating wavelength.

The phase-matching condition for a uniform fiber Bragg grating (FBG) with a period Λ is expressed by the equation $\beta_x - \beta_y = 2\pi/\Lambda$, where β_x and β_y represent the propagation constants of the forward and backward propagating modes, respectively. To achieve reflection within the same mode, it is necessary for the condition $\beta_x = -\beta_y$ to be satisfied. For a step-index multimode optical fiber, the propagation constant of the pth principal mode can be determined as follows [44]:

$$\beta_p = \frac{2\pi}{\lambda}\sqrt{n_2^2 + \psi_p N A^2} \tag{2}$$

where ψ_p represents the normalized propagation constant for the pth principal mode, and its value is determined by [45]

$$V = \frac{1}{\sqrt{1-\psi_p}}\left(p\frac{\pi}{2} + \frac{\pi}{4} + \arctan\left(\sqrt{\frac{\psi_p}{1-\psi_p}}\right)\right). \tag{3}$$

The positions of reflection peaks in FBGs are intricately determined by both the grating period and propagation constants. Manipulating the waveguide profiles of optical fibers allows for the precise adjustment of the spacing between these resonance peaks, facilitating the creation of multiwavelength filters. Throughout the fabrication process of these gratings, variations in refractive index and subtle deviations from perfect phase matching can induce shifts in the reflection peaks toward longer wavelengths, a phenomenon commonly referred to as a "red shift." Additionally, as the phase matching condition of a new mode approaches satisfaction, new reflection peaks may emerge; however, these peaks can be transient and may vanish with further irradiation. The amalgamation of multiple resonance peaks within FBGs results in a significantly broader bandwidth when compared to individual peaks, making them particularly well-suited for applications that demand wideband filters.

The characteristics of the grating within a multimode fiber can be assessed through the coupled-mode theory. This involves representing the overall electric field as a summation of the electric fields associated with the fiber modes, enabling the description of the behavior of the mth mode as it propagates along the z-axis. In the absence of Bragg gratings, the mode amplitude of the mth mode follows the coupled-mode equation as [46]

$$\frac{d\zeta_m}{d_z} = \sum_{n\neq m} -iC_{mn}\exp\left[-i\left(\beta_n - \beta_m + \frac{2\pi}{\Lambda}\right)z\right]\zeta_n \tag{4}$$

where ζ_m represents the mode amplitude of the mth mode; β_n, denoting the propagation constants; C_{mn}, signifying the

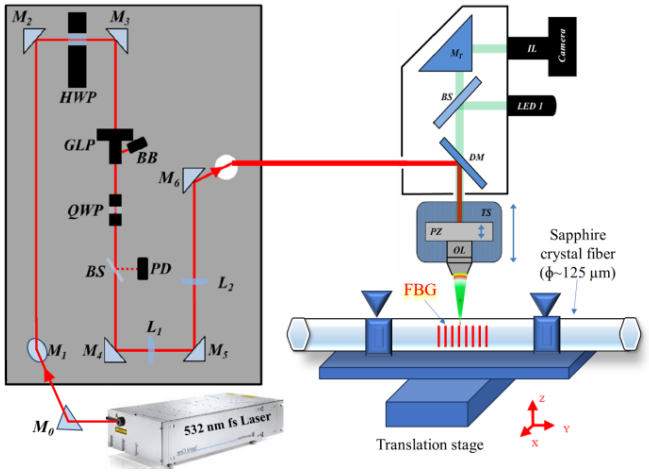

Fig. 1. Schematic of fs laser microfabrication system with M_0–M_6: mirrors, HWP: half-wave plate, GLP: Glan-laser polarizer, BB: beam block, QWP: quarter-wave plate, BS: beam sampler, PD: photodiode, L_1 and L_2: lens, DM: dichroic mirror, MT: turning mirror, IL: imaging lens system, OL: objective lens, PZ: piezo stage, and TS: translational stage.

coupling coefficient between modes m and n; and Λ stands for the grating period. As the detuning, computed as $\beta_m - \beta_n = 2\pi/\Lambda$, gradually diminishes toward zero, it signifies the successful fulfillment of the phase matching condition. The extent of coupling is directly dependent on the coupling coefficient between modes m and n. When modes m and n propagate in the same direction, this coupling coefficient is indicated as $C_{mn} = C_{mn}*$, with the asterisk symbolizing the complex conjugate. Conversely, when these modes travel in opposite directions, the coupling coefficient takes the form $C_{mn} = -C_{mn}*$. The specific value of this coupling coefficient, denoted as C_{mn}, can be determined through the methodology outlined in [47]

$$C_{mn} = \frac{\omega}{4}\iint \Delta\varepsilon(x,y,z)\overrightarrow{E_m}(x,y).\overrightarrow{E_n^*}(x,y)dxdy \tag{5}$$

where ε denotes the perturbation in permittivity, which can be approximated as $\varepsilon \approx 2n\delta n$, where δn is significantly smaller than n. Here, n represents the refractive index. The symbol ω corresponds to the optical frequency. The terms $\vec{E}(x,y)$ and $\vec{E_n^*}(x,y)$ represent the electric field distributions of modes m and n, respectively. These distributions are normalized to unit power, indicating the relative strength of the electric fields in each mode. The order of an FBG is given by [35], [43]

$$m\lambda_{\text{Bragg}} = 2n_{\text{eff}}\Lambda \tag{6}$$

where $m = 5$ corresponds to the order of FBG, and n_{eff} represents the effective refractive index of the fiber. Multimode fiber-based FBGs offer numerous benefits compared to their single-mode counterparts. These advantages stem from their larger mode field diameter and increased overlap between the modes and the grating, resulting in increased sensitivity to temperature and strain. Additionally, they can serve as distributed sensors for measuring temperature or strain along the fiber's length. However, it is important to note that modal interference and dispersion can introduce complexity into the analysis and impose limitations on FBG performance.

III. Experiment

A fs laser (Spirit One, Spectra-Physics) with pulse duration <400 fs at a repetition rate of 200 kHz was used for sapphire FBG inscription following a line-by-line laser scanning method. The laser system was integrated with an efficient second harmonic generation (SHG) module, which enabled switching the laser central wavelength between 520 and 1040 nm. The laser was customized to work at 520 nm at a 5-kHz repetition rate and 500 nJ/pulse. The custom-built fs-laser microfabrication system contains a fs laser and an automized workstation (femtoFBG, Newport Corporation), as shown in Fig. 1. The translation stage assembly (Newport, XMS100) included in the workstation provided a 3-D displacement accuracy of 0.05 μm across the x-axis and <1-nm resolution across the y- and z-axes. The average laser power was controlled by a half-wave plate and Glan-laser polarizer, built inside of femtoFBG workstation. The fs-laser pulses were reflected through a dichroic mirror and centered into the fiber using a 40X nonimmersion objective lens. The fiber alignment and FBG fabrication process were observed in real-time using a CMOS camera. The microfabrication system was controlled by a computer through a custom-built graphical user interface (GUI).

In this study, the effective refractive index (n_{eff}) for each Bragg wavelength is evaluated both experimentally and analytically using (6). In order to make strong FBG reflectors, a high pulse repetition rate and high laser intensity were employed, which led to a larger spot size, resulting in selecting a larger grating period. Higher order FBGs were fabricated to facilitate the laser spot size, and a grating period of 2.29 μm gave fifth-order FBGs with a Bragg wavelength of 1603.2 nm. Sapphire FBGs were fabricated in a 125-μm-diameter air clad, 30-cm-long sapphire fiber (MicroMaterials Inc, Tampa, FL, USA). One end of the sapphire fiber is a 0° polished end face in order to splice it to an MM silica fiber. The other end is 7° polished in order to eliminate endface reflections [26], [27]. The fabrication process was observed through a CMOS camera. To fabricate FBGs with 80 μm length, the origin (0,0,0) of the fabrication profile was set 12.5 μm away from the fiber boundary toward the longitudinal centerline of the fiber. The laser shutter opens, and the 3-D stage moves 80 μm along the negative x-axis direction, drawing an 80-μm line in the sapphire fiber. The laser shutter closes, and the stage moves along the y-axis direction to the point (0, 2.29 μm, 0). This process was repeated until the total moving distance along the positive y-axis reaches 7 mm, to the point (80 μm, 7000 μm, 0). The moving speed of the stage along the x-axis was 100 μm/s and along the y-axis was 1000 μm/s. The sapphire FBG was excited by connecting it to a 105-/125-μm multimode silica fiber using a mechanical splicer through a 50:50 multimode coupler. The signal from a high-power, broadband supercontinuum laser source (400–2000 nm) was launched into the multimode scrambler (MMS-201) and the output of the multimode scrambler was connected to the multimode coupler. The optical spectrum analyzer (OSA) collects the reflections from FBGs. The mode scrambler effectively randomizes the light from the laser source over time at a frequency of 150 kHz, so that the light distribution at the output was uniform and stationary, which helped reduce the multimodal interferences.

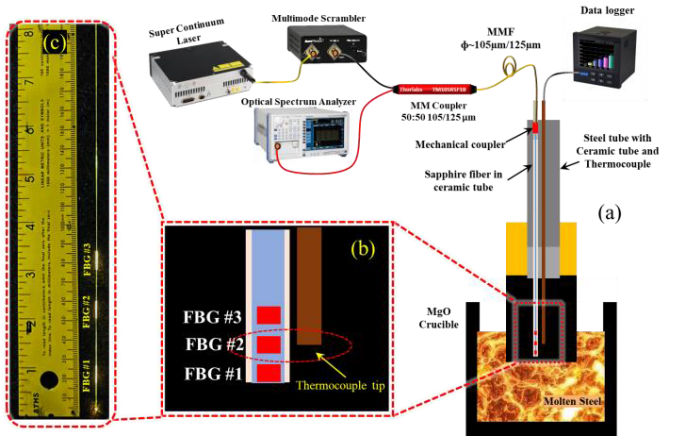

Fig. 2. First demonstration of sapphire FBGs in molten steel immersion test. (a) Schematic of FBG reflection spectrum measurement setup. (b) Enlarge inset shows sapphire FBG positions corresponding to a thermocouple. (c) Image of sapphire fiber showing FBG sections illuminated by the supercontinuum laser.

For the molten steel immersion test, a test frame with a motorized immersion and retraction mechanism was used to position the sample in the molten steel bath. A 200-lb. induction furnace capable of melting and holding steel at temperatures exceeding 1600 °C (3000 °F) for 30 min was used. The sapphire fiber was housed in a cylindrical sample tube made of alumina-graphite SEN refractory to measure the temperature gradient along the length of the sample. An S-type thermocouple was used for a reference temperature measurement for comparison. Fig. 2(a) shows the alumina graphite rod, which was 6" in height and 2" in diameter. A 0.5" diameter 5" deep hole was drilled to house the reference S-type thermocouple and the 18" long sapphire fiber with three inscribed FBGs.

The sapphire fiber was sheathed in an alumina tube of 0.219" OD × 0.156" ID to provide mechanical strength. A stainless-steel tube was connected to the ceramic tube using a high-temperature adhesive (JB Weld, 1000 °C) and was used to sheath the fiber and splice point up to the interrogation system. The wires of the S-type thermocouple were sheathed in a double-bore ceramic tube of 0. 125" OD × 0.04" ID. The fiber with FBGs was immersed into molten steel, such that two FBGs were below the molten steel and one FBG was above the melt. A schematic of this arrangement is shown in Fig. 2(a). Each FBG was 7 mm (0.28") long, across the longitudinal axis of the sapphire fiber. The spacing between the end face and FBG #1 was 12.7 mm. The space between FBG #1 and FBG #2 was 25 mm. The space between FBG #2 and FBG #3 was 15 mm. The thermocouple tip was placed next to FBG #2, as shown in Fig. 2(c). The placements of the FBGs and thermocouple tip were carefully aligned to measure a good temperature comparison between the thermocouple and FBG #2.

IV. Results and Discussion

The fabrication of FBG within a sapphire fiber was characterized by 80-μm line lengths, 2.29-μm grating periods, and an overall length of 7 mm. Microscopic images of the gratings, as depicted in Fig. 3(a) and (b), reveal the dimensions of

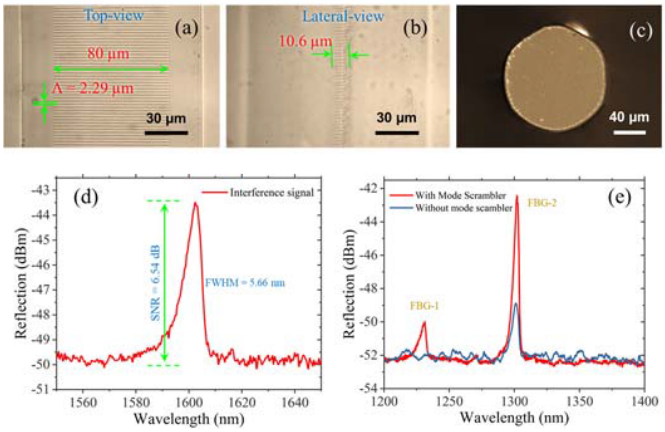

Fig. 3. Microscope images of a sapphire FBG. (a) Top view, (b) lateral view, (c) polished facet of sapphire crystal fiber, (d) sapphire FBG reflection spectrum, and (e) FBG reflection spectrum demonstrating mode scrambler efficiency.

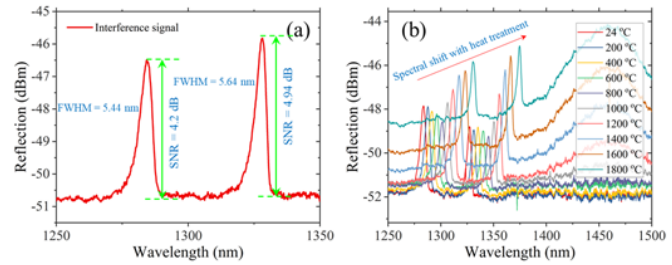

Fig. 4. Reflection spectra of two sapphire FBGs fabricated for high-temperature induction furnace tests. (a) Reflection spectra at room temperature (24 °C). (b) Sapphire FBG λ_{Bragg} increases by 7.2 nm for temperature increments of 200 °C up to 1800 °C.

80 μm in length (top view) and 10.6 μm in depth (lateral view). The polished sapphire crystal fiber can be seen in Fig. 3(c). The analysis of the reflection spectrum identified a peak with an SNR of 6.54 dB and an FWHM of 5.66 nm. To ensure uniform light distribution across the fiber's cross section and to mitigate mode-dependent losses and other distortions inherent in the multimode fiber optic system, a multimode scrambler was integrated into the sapphire fiber FBG light excitation pathway. This strategic intervention led to a more stable and uniform reflection spectrum, as illustrated in Fig. 3(d). The FBG reflection spectrum of a multimode step-index silica fiber (FG105LCA) with and without the implementation of a multimode scrambler is shown in Fig. 3(e), and it can be observed that the multimode scrambler (MMS-201) effectively increased SNR of FBGs and stabilized the baseline. The sapphire FBG was characterized in reflection mode for temperature measurement. The max reflectivity of the proposed FBG can be estimated by [48]

$$R = \tanh^2(C_{mn}.L) \tag{7}$$

where C_{mn} is the coupling coefficient (-0.0001612 μm^{-1}), L is the length of FBG (7 mm), and the reflectivity of the proposed sapphire FBG is obtained as ~10.38%.

Additionally, two new FBGs were fabricated on a 30-cm-long fiber with fiber length sufficient for installation in a heating furnace for observing the Bragg wavelength shift to temperature changes. Fig. 4(a) shows the reflection spectrum

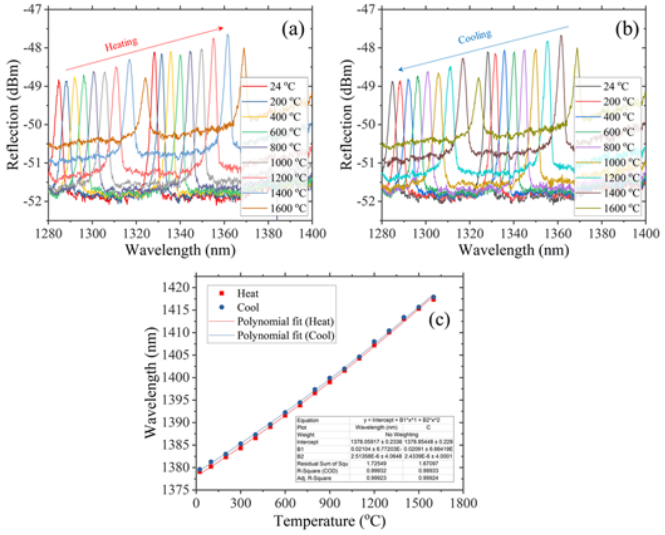

Fig. 5. Reflection spectra of sapphire FBGs as a function of temperature during (a) heating cycle, (b) cooling cycle, and (c) polynomial curve fit for sapphire FBG Bragg wavelength (λ_{Bragg}) versus temperature data for a heating and cooling cycle.

at room temperature (24 °C). The sapphire fiber with the FBG end was placed into a custom-built high-temperature induction furnace. The light scattered by the FBGs was used to fix the FBG position at the center of the furnace. The spectral response of the sapphire FBGs with varying temperatures up to 1800 °C is shown in Fig. 4(b). An increase in Bragg wavelength (λ_{Bragg}) with increasing temperature is expected and confirmed. The induction furnace temperature was monitored using an S-type thermocouple with a measurement range of 2000 °C. The fs-laser written gratings survived temperature exposure of 1800 °C for 45 min. For temperatures above 1400 °C, the SNR of the reflection peak diminished due to strong background light generated from the thermal radiation of the sapphire optical fiber. The use of a multimode scrambler helped in obtaining stable and accurate reflection spectra for various temperatures. Molten steel temperatures are typically around 1600 °C; hence, the spectrum shifts of the FBGs for heating and cooling cycles up to 1600 °C were observed, as shown in Fig. 5, and are of interest for additional high-temperature experiments.

Fig. 5(c) shows the wavelength change with increasing temperature and a polynomial curve fit with 99.93% accuracy for the heat cycle and 99.92% accuracy for the cool cycle. The plot of wavelength change with rising temperature shows a sensitivity of 33.55 pm/°C. A second-order polynomial fit curve is obtained for efficient wavelength to temperature conversion up to 1600 °C, as displayed in the inset of Fig. 5(c). The relationship between the change in sapphire FBG Bragg wavelength and change in temperature and strain can be obtained by [31], [34]

$$\Delta\lambda_{Bragg} = \lambda_{Bragg}(1 - p_e)\Delta\varepsilon + \lambda_{Bragg}(\alpha_S + \zeta_S)\Delta T. \tag{8}$$

The change in Bragg wavelength ($\Delta\lambda_{Bragg}$) is 49.77 nm at a reference wavelength λ_{Bragg} of 1603.2 nm without any applied strain, where the temperature was shifted from 28 °C to 1610 °C with an incremental trend. This temperature-induced wavelength shift closely aligns with the theoretical value of

TABLE I
SENSITIVITIES ESTIMATIONS OF THE PROPOSED SAPPHIRE FBG AT DIFFERENT WAVELENGTHS

λ	$\Delta\lambda$	S (pm/°C)	α_S	ζ_S	ΔT
1282	40.055	25.32	$7.15\times10^{-6}K^{-1}$	$12.6\times10^{-6}K^{-1}$	1582
1370	42.804	27.05	$7.15\times10^{-6}K^{-1}$	$12.6\times10^{-6}K^{-1}$	1582
1530	47.804	29.76	$7.15\times10^{-6}K^{-1}$	$12.6\times10^{-6}K^{-1}$	1582
1603	50.084	31.65	$7.15\times10^{-6}K^{-1}$	$12.6\times10^{-6}K^{-1}$	1582

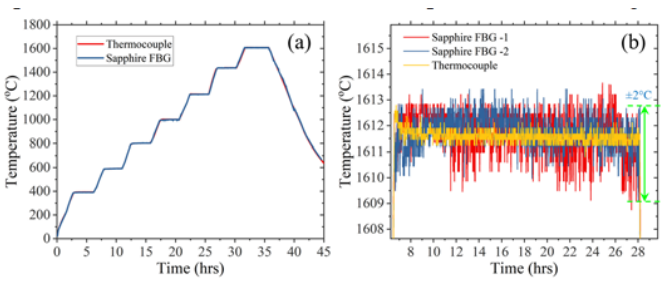

Fig. 6. Comparison of temperatures measured by sapphire FBGs and a thermocouple (S-type). (a) Various rise and hold temperatures in a heat cycle. (b) Temperature stability of ±2 °C for 22 h.

~50.084 nm, as calculated using (8), and the sensitivity of the sapphire FBG is obtained as 31.65 nm/°C. In this work, an experimental model has been established, allowing for the calculation of the theoretical sensitivity (S) of the proposed sapphire FBG at different Bragg wavelengths, namely, λ_{Bragg} ~ 1282, 1370, 1530, and 1603 nm. These theoretical sensitivity values are presented in Table I.

Furthermore, to perform a longer duration thermal stability analysis of the sapphire FBGs, the sapphire fiber with FBGs was inserted into a ceramic furnace (Criferon Model. SiC based). A 4 °C/min temperature ramp up was used to reach 1600 °C and FBG reflection spectra were recorded for 22 h to test FBG stability. The furnace temperature was controlled using an 80%–20% platinum–rhodium thermocouple and a second S-type thermocouple was placed close to one of the FBGs for temperature measuring comparisons.

Fig. 6(a) shows the comparison of temperatures measured by a thermocouple and a sapphire FBG. The reflection spectrum of the FBG is collected and is cross correlated with its preceding FBG spectrum. The difference in correlation is then used to calculate the FBG peak shift. A temperature ramp-up from room temperature to 1612 °C was performed between 0 and 6 h, followed by a temperature ramp down to room temperature after 28 h. The duration between 6 and 28 h indicates that the temperature was held at 1612 °C by the furnace. Thermal stability at 1612 °C for 22 h was observed, with less than a ±2 °C thermal drift for the sapphire FBG measured temperatures.

Fig. 6(b) shows a good match of temperature measured by the sapphire FBG and an S-type thermocouple for various hold and rise temperatures performed in a single heat cycle

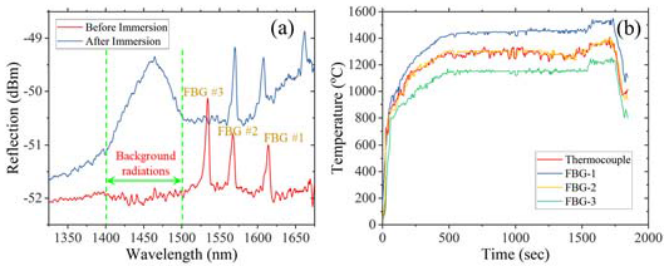

Fig. 7. First demonstration of sapphire FBG molten steel immersion. (a) Reflection spectra of sapphire FBGs before and during immersion. (b) Comparison of temperatures measured by the sapphire FBGs and the thermocouple (S-type).

demonstrating the accuracy of (8). Although the sapphire FBG (±2 °C) has slightly lower precision compared to a thermocouple (±0.5 °C), it offers distributed sensing capabilities, making it a highly cost-effective option over thermocouples. The sapphire fiber with FBG costs U.S. $260, whereas an S-type thermocouple costs U.S. $2000. Therefore, sapphire FBGs provide a more economical solution for distributed sensing applications.

For the molten steel immersion experiment, a single sapphire fiber with three FBGs was employed in the immersion setup shown in Fig. 2(b). Reflection spectra were recorded for 30 min during the immersion experiment. The reflection spectra of the FBGs before (at room temperature) and during immersion (at liquid steel temperature) are shown in Fig. 7(a). The background high-temperature thermal radiation peak can be observed in the 1400–1500-nm wavelength range along with the Bragg wavelength shifts of the inscribed FBGs. The comparisons of temperatures measured by the #2 sapphire FBG and the S-type thermocouple are shown in Fig. 7(b). It shows a close match between temperatures measured using FBG #2 and the nearby thermocouple. The FBGs placed below and above the liquid steel meniscus show a difference in temperature measurement as expected due to difference in thermal gradient. The sapphire fiber survived immersion into molten steel and successfully monitored temperatures along the alumina graphite sample tube for 30 min. The third-order polynomial transfer function developed above (2) facilitates accurate temperature measurements and the ceramic tube protects the sapphire fiber from contamination, making the sensors reusable.

V. CONCLUSION

Utilizing a fs laser, FBGs were inscribed within a sapphire optical fiber via a line-by-line scanning technique. This innovative approach yielded FBG reflection spectra boasting a remarkable SNR of 6.54 dB with low FWHM of 5.66 nm. The application of a mode scrambler (MMS-201) in an FBG demodulation system assisted in obtaining stable and accurate reflection spectra. The slender and well-defined Bragg wavelength peak facilitated highly efficient and precise temperature measurements, even in extreme environments exceeding 1600 °C. A rigorous thermal stability assessment of sapphire FBGs revealed temperature measurements characterized by a mere 0.125% error margin, coupled with a thermal drift within the range of ±2 °C. Notably, the inaugural implementation of sapphire FBGs in a molten steel immersion experiment

using an alumina-graphite SEN refractory provided compelling evidence of the efficacy of sapphire FBG sensors in successfully monitoring temperatures during this critical process. This groundbreaking achievement underscores the potential of sapphire FBG sensors as ideal candidates for integration into SENs and refractory linings. Furthermore, the superior efficiency and accuracy of sapphire FBG sensors, compared to traditional thermocouples, hold the promise of enhancing productivity, reducing power consumption, and diminishing the carbon footprint within the steel industry.

ACKNOWLEDGMENT

The views expressed herein do not necessarily represent the views of the U.S. Department of Energy or the United States Government.

REFERENCES

[1] L. Harrison. (2023). *AISI Releases Annual Statistical Report for 2022*. [Online]. Available: https://www.steel.org/2023/06/aisi-releases-annual-statistical-report-for-2022/#:~: text=The report highlights that%2C in,6.2 percent decrease from 2021

[2] K. Roy and M. Haresh. (2020). *Impacting Energy Through Smart Manufacturing*. [Online]. Available: https://www.automation.com/en-us/articles/december-2020/impacting-energy-through-smart-manufacturing

[3] R. Kashyap, *Fiber Bragg Gratings*. New York, NY, USA: Academic, 2009.

[4] J. Chen, B. Liu, and H. Zhang, "Review of fiber Bragg grating sensor technology," *Frontiers Optoelectron. China*, vol. 4, no. 2, pp. 204–212, Jun. 2011, doi: 10.1007/s12200-011-0130-4.

[5] X. Qiao, Z. Shao, W. Bao, and Q. Rong, "Fiber Bragg grating sensors for the oil industry," *Sensors*, vol. 17, no. 3, p. 429, Feb. 2017, doi: 10.3390/s17030429.

[6] D. Kinet, P. Mégret, K. Goossen, L. Qiu, D. Heider, and C. Caucheteur, "Fiber Bragg grating sensors toward structural health monitoring in composite materials: Challenges and solutions," *Sensors*, vol. 14, no. 4, pp. 7394–7419, Apr. 2014, doi: 10.3390/s140407394.

[7] J. Wans, D. Lieftucht, C. Geerkens, M. Arzberger, and M. Reifferscheid, "HD mold—Caster assistance system to increase product quality," in *Proc. AISTech-Iron Steel Technol. Conf.*, 2013, pp. 1385–1391.

[8] D. Lieftucht, M. Reifferscheid, T. Schramm, A. Krasilnikov, and D. Kirsch, "HD mold—A new fiber-optical-based mold monitoring system," *Iron Steel Technol.*, vol. 10, no. 12, pp. 87–95, 2013.

[9] E. Castiaux, and R. Belgium, "Use of FBG optical fibers in CC mould for BO detection and thermal exchange supervision," in Proc. 7th Int. Congr. Sci. Technol. Steelmaking, Challenge Ind. 4.0 (ICS), 2018.

[10] T. Spierings, A. Kamperman, H. Hengeveld, J. Kromhout, and E. Dekker, "Development and application of fiber Bragg gratings for slab casting," in *Proc. AISTech-Iron Steel Technol. Conf.*, 2017, pp. 1655–1663.

[11] J. He, B. Xu, X. Xu, C. Liao, and Y. Wang, "Review of femtosecond-laser-inscribed fiber Bragg gratings: Fabrication technologies and sensing applications," *Photonic Sensors*, vol. 11, no. 2, pp. 203–226, Jun. 2021, doi: 10.1007/s13320-021-0629-2.

[12] S. J. Mihailov, "Fiber Bragg grating sensors for harsh environments," *Sensors*, vol. 12, no. 2, pp. 1898–1918, Feb. 2012, doi: 10.3390/s120201898.

[13] S. Mihailov et al., "Extreme environment sensing using femtosecond laser-inscribed fiber Bragg gratings," *Sensors*, vol. 17, no. 12, p. 2909, Dec. 2017, doi: 10.3390/s17122909.

[14] C. R. Liao and D. N. Wang, "Review of femtosecond laser fabricated fiber Bragg gratings for high temperature sensing," *Photon. Sensors*, vol. 3, no. 2, pp. 97–101, Jun. 2013, doi: 10.1007/s13320-012-0060-9.

[15] S. J. Mihailov, D. Grobnic, C. W. Smelser, P. Lu, R. B. Walker, and H. Ding, "Bragg grating inscription in various optical fibers with femtosecond infrared lasers and a phase mask," *Opt. Mater. Exp.*, vol. 1, no. 4, p. 754, 2011.

[16] C. Zhu, D. Alla, and J. Huang, "High-temperature stable FBGs fabricated by a point-by-point femtosecond laser inscription for multi-parameter sensing," *OSA Continuum*, vol. 4, no. 2, p. 355, Feb. 2021, doi: 10.1364/osac.415685.

[17] S. Yang et al., "Application of sapphire-fiber-Bragg-grating-based multi-point temperature sensor in boilers at a commercial power plant," *Sensors*, vol. 19, no. 14, p. 3211, Jul. 2019, doi: 10.3390/s19143211.

[18] B. Wang, Y. Niu, X. Qin, Y. Yin, and M. Ding, "Review of high temperature measurement technology based on sapphire optical fiber," *Measurement*, vol. 184, Nov. 2021, Art. no. 109868, doi: 10.1016/j.measurement.2021.109868.

[19] C. Zhu, R. E. Gerald, and J. Huang, "Progress toward sapphire optical fiber sensors for high-temperature applications," *IEEE Trans. Instrum. Meas.*, vol. 69, no. 11, pp. 8639–8655, Nov. 2020, doi: 10.1109/TIM.2020.3024462.

[20] C. Liu, S. Tsai, C. Ni, K. Fung, and C. Cho, "Enhancement on densification and crystallization of conducting $La_{0.7}Sr_{0.3}VO_3$ perovskite anode derived from hydrothermal process," *Jpn. J. Appl. Phys.*, vol. 58, no. SD, p. DG03, 2019, doi: 10.7567/1347-4065/ab0df0.

[21] Y. B. Yu and W. K. Chow, "Review on an advanced high-temperature measurement technology: The optical fiber thermometry," *J. Thermodyn.*, vol. 2009, pp. 1–11, Jan. 2009, doi: 10.1155/2009/823482.

[22] J. Qian et al., "Machine learning-assited optical thermometer for continuous temperature analysis inside molten metal," *Sens. Actuators A, Phys.*, vol. 322, May 2021, Art. no. 112626, doi: 10.1016/j.sna.2021.112626.

[23] T. Habisreuther, T. Elsmann, Z. Pan, A. Graf, R. Willsch, and M. A. Schmidt, "Sapphire fiber Bragg gratings for high temperature and dynamic temperature diagnostics," *Appl. Thermal Eng.*, vol. 91, pp. 860–865, Dec. 2015, doi: 10.1016/j.applthermaleng.2015.08.096.

[24] S. Yang, D. Homa, G. Pickrell, and A. Wang, "Fiber Bragg grating fabricated in micro-single-crystal sapphire fiber," *Opt. Lett.*, vol. 43, no. 1, p. 62, Jan. 2018, doi: 10.1364/ol.43.000062.

[25] C. Hill et al., "Single mode air-clad single crystal sapphire optical fiber," *Appl. Sci.*, vol. 7, no. 5, p. 473, May 2017, doi: 10.3390/app7050473.

[26] M. Busch, W. Ecke, I. Latka, D. Fischer, R. Willsch, and H. Bartelt, "Inscription and characterization of Bragg gratings in single-crystal sapphire optical fibres for high-temperature sensor applications," *Meas. Sci. Technol.*, vol. 20, no. 11, Nov. 2009, Art. no. 115301, doi: 10.1088/0957-0233/20/11/115301.

[27] T. Elsmann et al., "High temperature sensing with fiber Bragg gratings in sapphire-derived all-glass optical fibers," *Opt. Exp.*, vol. 22, no. 22, p. 26825, Nov. 2014, doi: 10.1364/oe.22.026825.

[28] X. Xu, J. He, C. Liao, and Y. Wang, "Multi-layer, offset-coupled sapphire fiber Bragg gratings for high-temperature measurements," *Opt. Lett.*, vol. 44, no. 17, p. 4211, Sep. 2019, doi: 10.1364/ol.44.004211.

[29] X. Xu et al., "Sapphire fiber Bragg gratings inscribed with a femtosecond laser line-by-line scanning technique," *Opt. Lett.*, vol. 43, no. 19, p. 4562, Oct. 2018, doi: 10.1364/ol.43.004562.

[30] D. Grobnic, S. J. Mihailov, C. W. Smelser, and H. Ding, "Sapphire fiber Bragg grating sensor made using femtosecond laser radiation for ultrahigh temperature applications," *IEEE Photon. Technol. Lett.*, vol. 16, no. 11, pp. 2505–2507, Nov. 2004, doi: 10.1109/lpt.2004.834920.

[31] Q. Guo et al., "Femtosecond laser inscribed sapphire fiber Bragg grating for high temperature and strain sensing," *IEEE Trans. Nanotechnol.*, vol. 18, pp. 208–211, 2019, doi: 10.1109/TNANO.2018.2888536.

[32] S. Yang, D. Hu, and A. Wang, "Point-by-point fabrication and characterization of sapphire fiber Bragg gratings," *Opt. Lett.*, vol. 42, no. 20, p. 4219, Oct. 2017, doi: 10.1364/ol.42.004219.

[33] H. Chen, M. Buric, P. R. Ohodnicki, J. Nakano, B. Liu, and B. T. Chorpening, "Review and perspective: Sapphire optical fiber cladding development for harsh environment sensing," *Appl. Phys. Rev.*, vol. 5, no. 1, Mar. 2018, Art. no. 011102, doi: 10.1063/1.5010184.

[34] S. J. Mihailov, D. Grobnic, and C. W. Smelser, "High-temperature multiparameter sensor based on sapphire fiber Bragg gratings," *Opt. Lett.*, vol. 35, no. 16, p. 2810, 2010.

[35] F. Mumtaz, H. Tekle, B. Zhang, J. D. Smith, R. J. O'Malley, and J. Huang, "Highly cascaded first-order sapphire optical fiber Bragg gratings fabricated by a femtosecond laser," *Opt. Lett.*, vol. 48, no. 16, p. 4380, 2023, doi: 10.1364/ol.495138.

[36] F. Mumtaz, B. Zhang, R. J. O'Malley, and J. Huang, "Large-scale cascading of first-order FBG array in a highly multimode coreless fiber using femtosecond laser for distributed thermal sensing," *Opt. Exp.*, vol. 31, no. 18, pp. 29639–29653, 2023.

[37] F. Mumtaz, H. Tekle, B. Zhang, J. D. Smith, R. J. O'Malley, and J. Huang, "Highly cascaded first-order sapphire optical fiber Bragg gratings fabricated by a femtosecond laser," *Opt. Lett.*, vol. 48, no. 16, pp. 4380–4383, 2023.

[38] A. Yariv and P. Yeh, "Guided waves and integrated optics," in *Optical Waves in Crystals*. Hoboken, NJ, USA: Wiley, 2002, ch. 11, pp. 417–516.
[39] Y. Lai, Y. Yu, S. Fu, J. Xu, P. P. Shum, and X. Zhang, "Efficient spot size converter for higher-order mode fiber-chip coupling," *Opt. Lett.*, vol. 42, no. 18, p. 3702, 2017, doi: 10.1364/ol.42.003702.
[40] W. E. S. Hen, J. D. U. Iangbing, and Z. H. E. Uyuan, "Coupler for 2 × 100 Gbps/Lambda MDM optical interconnection," *Opt Exp.*, vol. 28, no. 22, pp. 33254–33262, 2020.
[41] F. Mumtaz, M. A. Ashraf, Y. Dai, and W. Hu, "Numerical solution of strongly guided modes propagating in sapphire crystal fibers (α-Al_2O_3) for UV, VIS/IR wave-guiding," *Results Phys.*, vol. 18, Sep. 2020, Art. no. 103311, doi: 10.1016/j.rinp.2020.103311.
[42] F. Mumtaz, Y. Dai, M. A. Ashraf, and W. Hu, "A star-wheel design of single crystal sapphire optical fiber promoting single mode operation in the infrared regime," *Prog. Electromagn. Res. C*, vol. 107, pp. 219–231, 2021, doi: 10.2528/pierc20111905.
[43] F. Mumtaz et al., "Thermally robust and highly stable method for splicing silica glass fiber to crystalline sapphire fiber," *Appl. Opt.*, vol. 62, no. 5, p. 1392, 2023, doi: 10.1364/AO.479732.
[44] K. H. Wanser, K. F. Voss, and A. D. Kersey, "Novel fiber devices and sensors based on multimode fiber Bragg gratings," in *Proc. 10th Int. Conf. Opt. Fibre Sensors*, Sep. 1994, pp. 265–268, doi: 10.1117/12.185051.
[45] X. Sang, C. Yu, and B. Yan, "Bragg gratings in multimode optical fibers and their applications," *J. Optoelectron. Adv. Mater.*, vol. 9, no. 8, pp. 2356–2361, 2007.
[46] O. Katsunari, "Coupled mode theory," in *Fundamentals of Optical Waveguides*, 2nd ed. New York, NY, USA: Academic, 2006, ch. 4.
[47] J. Zhang, H. Yu, C.-Q. Xu, and W.-P. Huang, "Multimode optical fiber Bragg gratings: Modeling, simulation, and experiments," *Proc. SPIE*, vol. 5579, pp. 435–442, Nov. 2004, doi: 10.1117/12.567283.
[48] K. Porsezian and K. Senthilnathan, *Guided Wave Optical Components and Devices: Solitons in a Fiber Bragg Grating*. New York, NY, USA: Academic, 2006, ch. 17, doi: 10.1016/B978-012088481-0/50018-8.

Dinesh Reddy Alla received the B.Tech. degree in electronics and communication engineering from Jawaharlal Nehru Technological University, Kakinada, India, in 2014, the M.S. and Ph.D. degrees in electrical engineering from the Missouri University of Science and Technology, Rolla, MO, USA, in 2017 and 2023, respectively.

His current research interests include distributed fiber-optic sensors for temperature and strain measurements.

Deva Prasad Neelakandan received the B.E. degree in mechanical engineering from the Sri Shakthi Institute of Engineering and Technology, Coimbatore, India, in 2016, and the M.S. degree in mechanical engineering from the Missouri University of Science and Technology, Rolla, MO, USA, in 2018. He is currently pursuing the Ph.D. degree in material science and engineering with Auburn University, Auburn, AL, USA.

His research interests include the instrumentation of optical fiber for temperature and strain measurements in steel-based applications.

Farhan Mumtaz (Member, IEEE) received the bachelor's degree in science from Punjab University Lahore, Lahore, Pakistan, in 2006, the master's degree in electronics from Quaid-i-Azam University Islamabad, Islamabad, Pakistan, in 2018, and the Ph.D. degree in information and communication engineering from the Wuhan University of Technology, Wuhan, China, in 2021.

In February 2022, he starts working with the Faculty of Electrical and Computer Engineering, Missouri University of Science and Technology, Rolla, MO, USA, where he is currently as an Assistant Research Professor. From 2007 to 2015, he worked for Huawei Technologies (Pvt.) Ltd., Islamabad, Pakistan, holding a number of important positions, including a Plan Control Manager, a Project Manager, and a Service Solution Manager. His current research interests include sapphire crystalline fibers, fiber Bragg gratings, femtosecond micromachining of optoelectronic materials, Rayleigh and Brillion sensors, surface plasmons, biosensors, photonic crystal fiber design, and instrumentation of fiber optic sensors for energy and harsh environments in U.S. steelmaking industry.

Rex E. Gerald II received the B.A. degree (Hons.) in chemistry from The University of Chicago (UC), Chicago, IL, USA, in 1984, and a conjoint Ph.D. degree in physical chemistry from the University of Illinois Chicago (UIC), Chicago, and the Max Planck Institute (MPI), Heidelberg, Germany, in 1994.

He is currently a Research Professor with the Lightwave Technology Laboratory, Department of Electrical and Computer Engineering, Missouri University of Science and Technology (MS&T), Rolla, Mo, USA. He holds 26 U.S. patents and coauthored more than 50 publications from research investigations conducted at UC, UIC, MPI, Argonne National Laboratory, and MS&T.

Laura Bartlett is currently the Robert V. Wolf Endowed Professor of metallurgical engineering and the Foundry Educational Foundation Key Professor of metal casting technology with the Missouri University of Science and Technology, Rolla, MO, USA. She is the Director of the Robert V. Wolf Educational and Research Foundry, Missouri University of Science and Technology and the Thermal Processing Laboratory. Her teaching and research experiences are in the areas of foundry steelmaking and the physical metallurgy of iron and steel casting alloys. Her work on the development of advanced high-strength and lightweight steels for military vehicles is currently funded by the Department of Defense through organizations, such as the Army Research Laboratory and Defense Logistics Agency. She has coauthored more than 40 peer-reviewed articles. Her current research interests include the inclusion engineering and solidification phenomena in high-strength steels, the experimental and theoretical aspects of phase transformations, microstructure mechanical property relationships in high-strength alloys, and the development of advanced high-strength and lightweight steels.

Ms. Bartlett has won several awards of distinction for her research including seven best paper awards and three research and professional development awards.

Ronald J. O'Malley is currently the F. Kenneth Iverson Chair Professor of Steelmaking Technologies with the Department of Metallurgical Engineering, Missouri University of Science and Technology, Rolla, MO, USA. He is also the Director of the Kent D. Peaslee Steel Manufacturing Research Center (PSMRC), which is an industry-supported consortium with 18 industry members that support >U.S. $850k in research annually. He is also the PI for >U.S. $18M in research with the Department of Energy (DOE) in areas of sensor development, hydrogen steelmaking, and electric furnace optimization and is a Lecturer for several short courses in steel manufacturing, including the Brimacombe short course on continuous casting. He has more than 30 years of experience in the metals manufacturing industry at Alcoa, Alcoa Center, New Kensington, PA, USA, Armco/AK Steel, Middletown, OH, USA, and Nucor Steel, LLC, Decatur, AL, USA. He has authored more than 150 journal and conference proceedings papers, over 70 invited and contributed presentations, and holds three U.S. patents. His current research interests include H2 Ironmaking, EAF steelmaking, steel refining, clean steel processing and inclusion engineering, steel-refractory interactions, continuous casting, deformation processing, sensor development for harsh steelmaking environments, and new steel grade development.

Mr. O'Malley is an AIST Distinguished Member and a fellow. He was the President of the Association for Iron and Steel Technology (AIST) from 2019 to 2021. He is currently serving on the executive board for AIST.

Jeffrey D. Smith is currently a Professor of ceramic engineering with the Department of Materials Science and Engineering, Missouri University of Science and Technology, Rolla, MO, USA. His current research interests include high-temperature inorganic chemistry, materials characterization, high-temperature materials, and interactions between ceramics and molten materials.

Jie Huang (Senior Member, IEEE) received the Ph.D. degree in electrical engineering from Clemson University, Clemson, SC, USA, in 2015.

He is currently the Roy A. Wilkens Endowed Associate Professor of electrical and computer engineering with the Missouri University of Science and Technology, Rolla, MO, USA. He has established the Lightwave Technology Laboratory (LTL), Rolla, with a strong track record of sustained research funding, high-quality journal publications, and the state-of-the-art research infrastructures with cutting-edge capabilities. He has authored or coauthored over 100 refereed articles, 70 conference papers, one book chapter, and ten U.S. patent applications, all in the arena of advanced sensors. His current research interests include the development of optical and microwave sensors and instrumentation for applications in energy, intelligent infrastructures, clean environments, biomedical sensing, and harsh environments.